Soft Matter

Enhancement of the Mechanical Properties of Organic–Inorganic Hybrid Elastomers by Introducing Movable and Reversible Crosslinks

Journal:	*Soft Matter*
Manuscript ID	SM-ART-08-2023-001101.R2
Article Type:	Paper
Date Submitted by the Author:	04-Nov-2023

Complete List of Authors:	Yamashita, Naoki; Graduate School of Science, Osaka University, Department of Macromolecular Science Yamaoka, Kenji; Graduate School of Science, Osaka University, Department of Macromolecular Science; Forefront Research Center, Graduate School of Science, Osaka University Ikura, Ryohei; Graduate School of Science, Osaka University, Department of Macromolecular Science; Forefront Research Center, Graduate School of Science, Osaka University Yoshida, Daichi; Graduate School of Science, Osaka University, Department of Macromolecular Science Park, Junsu; Graduate School of Science, Osaka University, Department of Macromolecular Science; Forefront Research Center, Graduate School of Science, Osaka University Kato, Nobu; Shinetsu Kagaku Kogyo Kabushiki Kaisha Kamei, Masayuki; Shin-etsu Chemical Co Ltd Ogura, Kentaro; Shinetsu Kagaku Kogyo Kabushiki Kaisha Igarashi, Minoru; Shinetsu Kagaku Kogyo Kabushiki Kaisha Nakagawa, Hideo; Shin-etsu Chemical Co Ltd Takashima, Yoshinori; Graduate School of Science, Osaka University, Department of Macromolecular Science; Forefront Research Center, Graduate School of Science, Osaka University; Innovative Catalysis Science Division, Institute for Open and Transdisciplinary Research Initiatives (ICS-OTRI), Osaka University

ARTICLE

Enhancement of the Mechanical Properties of Organic–Inorganic Hybrid Elastomers by Introducing Movable and Reversible Crosslinks

Received 00th January 20xx,
Accepted 00th January 20xx

DOI: 10.1039/x0xx00000x

≠Naoki Yamashita,[a] ≠Kenji Yamaoka,[a,b] Ryohei Ikura,[a,b] Daichi Yoshida,[a] Junsu Park,[a,b] Nobu Kato,[c] Masanao Kamei,[c] Kentaro Ogura,[c] Minoru Igarashi,[c] Hideo Nakagawa,[d] and Yoshinori Takashima[a,b,e]* (≠ Contributed equally to this work)

Organic–inorganic materials have been widely utilized in various fields because of their multifunctional materials. Poly (dimethyl siloxane) (PDMS), a typical inorganic polymer, has industrially appealing functions, such as transparency, biocompatibility, and gas permeability; however, it has poor mechanical properties. We incorporated organic–inorganic hybrid elastomers (PDMS-γCD-AAl ⊃ P(EA-HEMA) (*x*)) with movable crosslinks, and we utilized hydrogen bonds as reversible crosslinks. The organic polymer poly ethyl acrylate-r-hydroxy ethyl methacrylate (P(EA-HEMA)) penetrated the cavity of triacetylated γ-cyclodextrin (γCD), which was introduced into the side chains of PDMS, and it compounded with PDMS at the nanoscale. Structural studies involving visual and X-ray scattering measurements revealed that movable crosslinks improved the compatibility levels of PDMS and acrylate copolymers. However, macroscopic phase separation occurred when the number of reversible crosslinks increased. Furthermore, studies on the mobility levels of acrylate copolymers and movable crosslinks indicated that the relaxation behaviour of PDMS-γCD-AAl ⊃ P(EA-HEMA) (*x*) changed with changing numbers of reversible crosslinks. Introducing reversible crosslinks improved the Young's modulus and toughness values. The movable and reversible crosslinks between the organic and inorganic polymers contributed to the high elongation properties. The design of PDMS-γCD-AAl ⊃ P(EA-HEMA) (*x*) incorporated cooperatively movable and reversible crosslinks to achieve highly compatible of immiscible polymers and to control the mechanical properties.

1. Introduction

Organic–inorganic hybrid materials have been widely applied to explore new materials and their specific features[1-3]. Generally, inorganic fillers, such as clay[4-7], silica particles[8-10], metal nanoparticles[11-13], and polyhedral oligomeric silsesquioxanes[14-20], have been used as composite materials when combined with organic polymers. Polydimethylsiloxane (PDMS), an inorganic polymer, has excellent heat resistance[21-23], transparency[24,25], biocompatibility[26,27], and gas permeability[28,29] characteristics; however, its mechanical properties are inferior to those of common organic polymers[30]. The mechanical properties of PDMS have been improved by introducing various crosslinks and intermolecular interactions[31-40]. We have reported an improvement in the mechanical properties of PDMS-incorporated topological crosslinks with cyclodextrin (CD)[41,42]. We have succeeded in improving the compatibility and toughness characteristics by compositing immiscible polymers with movable crosslinks; in these systems, the main chain penetrates the CD cavity[43-46]. We hypothesize that if the organic polymer and PDMS can be crosslinked by movable crosslinks, each function will be combined and the mechanical properties will be improved. In this study, we propose the enhancement of mechanical properties of a polymer blend with the topological and reversible crosslinking design between dissimilar polymers. Compared to previously reported copolymerization[47] or interpenetrating[48] of organic and inorganic polymers for composites, our crosslinking design moderately constrains the chain mobility. We consider that a polymer blend of organic polymers and PDMS with the topological and reversible crosslinks can be used to construct the function of organic–inorganic hybrid materials, such as the miscibility and toughening, controlling the chain mobility.

Herein, we prepare PDMS modified with γCDs (PDMS-γCD-AAl) to form movable crosslinks, and we composite it with ethyl acrylate-co-hydroxy ethyl acrylate polymers (PDMS-γCD-AAl ⊃ P(EA-HEMA)). Furthermore, by forming reversible crosslinks based on hydrogen bonds (H-bonds) between PDMS-γCD-AAl and P(EA-HEMA), intermolecular H-bonds control the mechanical properties of PDMS-γCD-AAl ⊃ P(EA-HEMA) (**Fig. 1**).

[a] *Department of Macromolecular Science, Graduate School of Science, Osaka University, 1-1 Machikaneyamacho, Toyonaka, Osaka 560-0043, Japan.*
[b] *Forefront Research Center, Graduate School of Science, Osaka University,1-1 Machikaneyamacho, Toyonaka, Osaka 560-0043, Japan.*
[c] *Shin-Estu Chemical Co., Ltd., Silicone-Electronics Materials Research Center, 1-10, Hitomi, Matsuida-machi, Annaka-shi, Gunma 379-0224, Japan.*
[d] *Shin-Etsu Chemical Co., Ltd., 4-1 Marunouchi, 1 chome, Chiyoda-ku, Tokyo 100-0005, Japan.*
[e] *Innovative Catalysis Science Division, Institute for Open and Transdisciplinary Research Initiatives, Osaka University, 1-1 Yamadaoka, Suita, Osaka 565-0871, Japan.*
†Electronic Supplementary Information (ESI) available. See
DOI: 10.1039/x0xx00000x

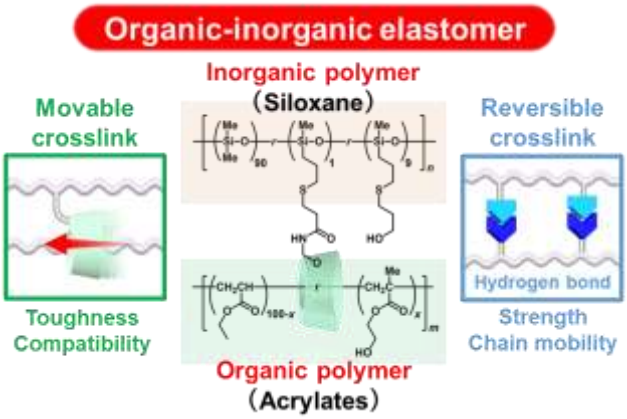

Fig. 1 Concept image of organic–inorganic hybrid elastomers (PDMS-γCD-AAl ⊃ P(EA-HEMA) (*x*)) by introducing movable and reversible crosslinks.

2. Results and discussion

2.1. Preparation of organic–inorganic hybrid elastomer

TAcγCD-modified PDMS was prepared via a thiol-ene reaction between triacetylated 6-acrylamido methylether-γ-cyclodextrin (TAcγCDAAmMe) and thiol modified PDMS (PDMS-SH) in the presence of allyl alcohol (AAl) to protect the residual thiol groups (PDMS-γCD-AAl) (**Fig. 2a**). **Scheme S1** shows the details of the synthesis of PDMS-γCD-AAl. Proton nuclear magnetic resonance (^{1}H NMR) measurements of PDMS-γCD-AAl showed that the mol% contents of γCD and AAl among all repeating units were 1 and 9, respectively (**Fig. S1**).

The knitting methods with PDMS-γCD-AAl serving as the primary polymer and acrylate polymers serving as the secondary polymer yielded an organic–inorganic hybrid elastomer (PDMS-γCD-AAl ⊃ P(EA-HEMA) (*x*)), where *x* is the mol% content of a H-bond moiety in the acrylate copolymer (**Fig. 2b**). PDMS-γCD-AAl ⊃ P(EA-HEMA) (*x*) was obtained by conducting solution polymerization on the second main-chain acrylate monomers at each concentration in the PDMS-γCD-AAl solution (**Scheme S2 and Table S1**). In this study, ethyl acetate was chosen as the reaction solvent to modify PDMS with γCD and allyl alcohol groups. We chose ethyl acrylate (EA) and 2-hydroxyethyl methacrylate (HEMA) as the acrylate monomers. Acrylate copolymers with different compositions of EA and HEMA were used as secondary polymers (P(EA-HEMA) (*x*)). The HEMA unit formed a H-bond with AAl in PDMS-γCD-AAl. Varying the amount of HEMA controlled the H-bonds between PDMS-γCD-AAl and P(EA-HEMA). ^{1}H NMR spectra confirmed the desired polymer structure

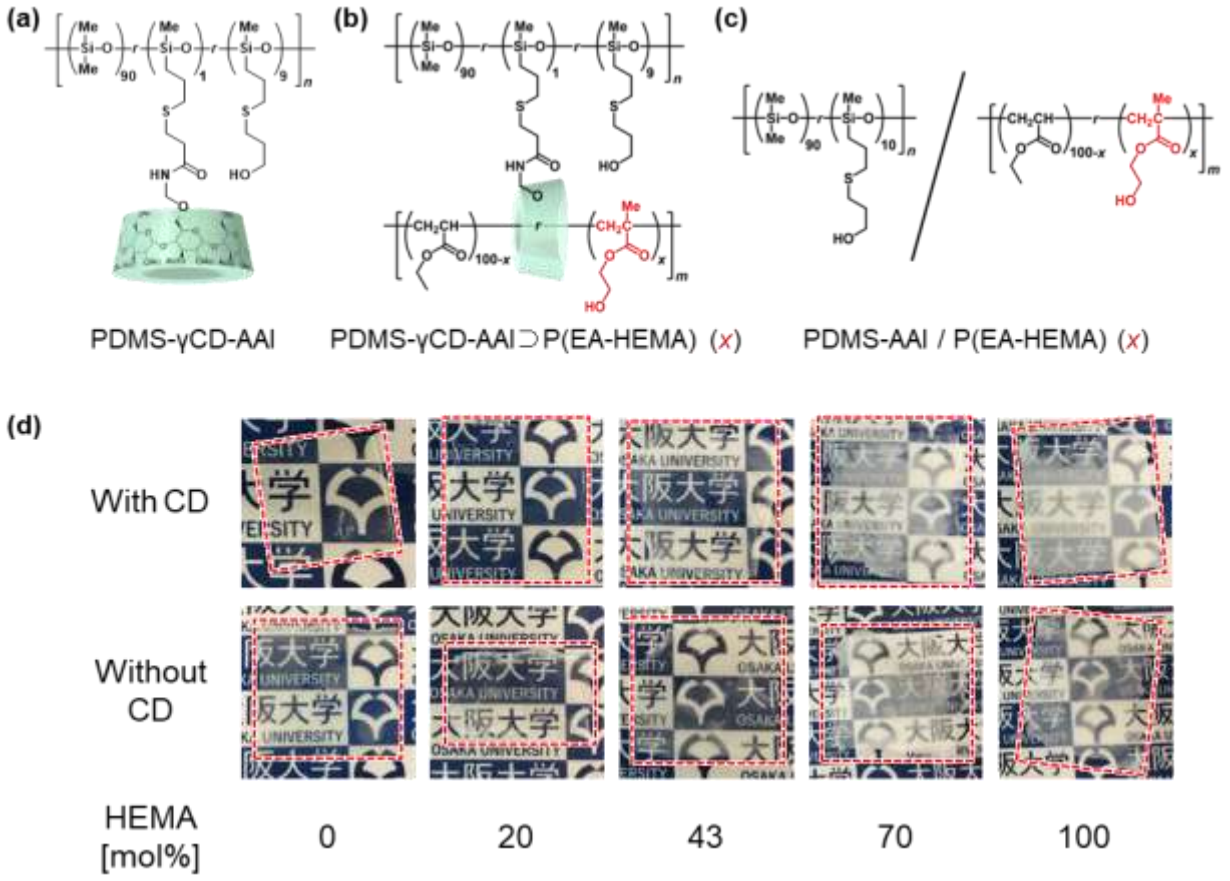

Fig. 2 Chemical structures of (**a**) PDMS-γCD-AAl, (**b**) PDMS-γCD-AAl ⊃ P(EA-HEMA) (*x*), and (**c**) PDMS-AAl/P(EA-HEMA) (*x*) blends without movable crosslinks. *x* is the mol% HEMA content in acrylate copolymers. (**d**) Photographs of PDMS-γCD-AAl ⊃ P(EA-HEMA) (*x*) and PDMS-AAl/P(EA-HEMA) (*x*).

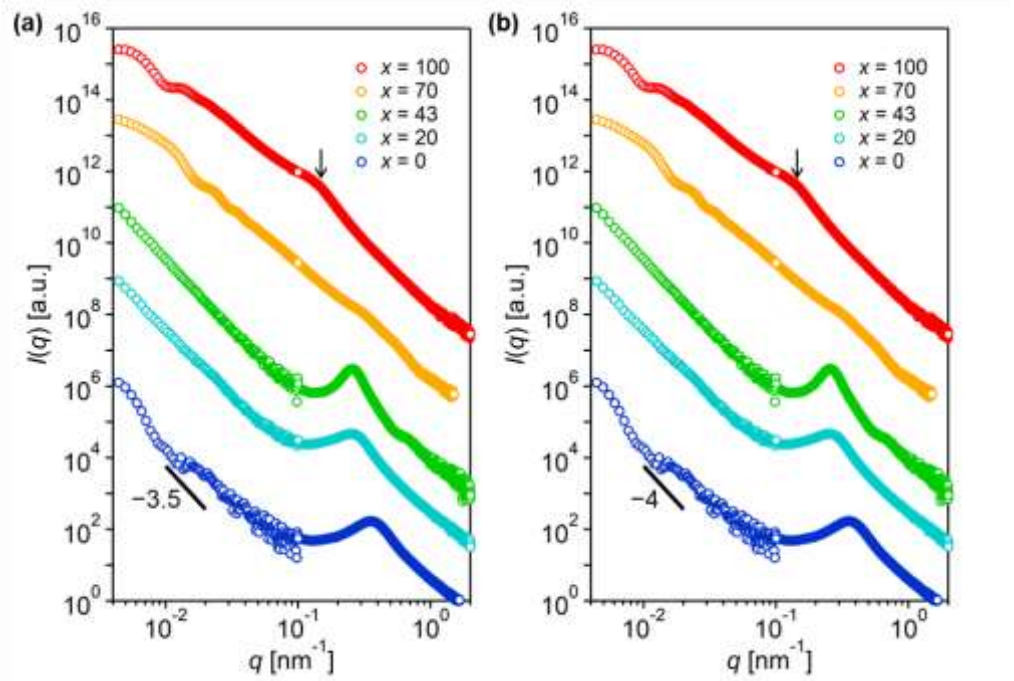

Fig. 3 USAXS and SAXS profiles of (a) PDMS-γCD-AAl ⊃ P(EA-HEMA) (*x*) and (b) PDMS-AAl/P(EA-HEMA) (*x*).

(**Fig. S3–7**). The PDMS-γCD-AAl and P(EA-HEMA) were immobilized at weight ratios of 1:1. The γCD units formed movable crosslinks between the acrylate chains. PDMS-AAl and P(EA-HEMA) (*x*) blends (PDMS-AAl/P(EA-HEMA) (*x*)) without movable crosslinks of γCD were used as negative control samples (**Fig. 2c**). PDMS-AAl/P(EA-HEMA) (*x*) was prepared with the same procedure used for the synthesis of PDMS-γCD-AAl ⊃ P(EA-HEMA) (*x*) (**Scheme S3**). This procedure confirmed the desired polymer structures (**Fig. S8–12**).

Fig. 2d shows photographs of the elastomer films of PDMS-γCD-AAl ⊃ P(EA-HEMA) (*x*) and PDMS-AAl/P(EA-HEMA) (*x*). The elastomer films with γCD were colourless and transparent when *x* was less than 20, but they became white and turbid above *x* = 43. As the composition of HEMA increased, the modified PDMS and acrylate copolymers caused phase separation because HEMA had a lower solubility in ethyl acetate than EA. The elastomer films without γCD became turbid for all compositions. The movable crosslinks improved the compatibility between the modified PDMS and acrylate copolymers.

2.2. Internal structures of the hybrid materials

We conducted ultrasmall-angle X-ray scattering (USAXS) and small-angle X-ray scattering (SAXS) to evaluate the phase-separated structures of PDMS-γCD-AAl ⊃ P(EA-HEMA) (*x*) and PDMS-AAl/P(EA-HEMA) (*x*). We combined the USAXS and SAXS profiles at the scattering vector $q = 10^{-1}$ nm^{-1} to obtain a comprehensive understanding over a wide range of scales (**Fig. 3**). By considering the relatively large scale measured by USAXS ($q < 10^{-1}$ nm^{-1}), we discuss the macro-scale phase structure cause the haze of film samples. The scattering intensity of PDMS-γCD-AAl ⊃ P(EA-HEMA) (*x*) decayed with $q^{-3.5}$ at a relatively low *x*. PDMS-γCD-AAl ⊃ P(EA-HEMA) (*x*) exhibited characteristic scattering from spherical structures at relatively high *x* values (**Fig. 3a**). The spherical structure of the scatterer caused turbidity of the elastomer film with a high HEMA content. The scattering intensity of PDMS-AAl/P(EA-HEMA) (*x*) followed Porod's law, decaying with q^{-4} at a relatively low *x*; this intensity suggested the presence of macroscopic phase separation, exhibiting a sharp interface between PDMS and acrylate copolymers (**Fig. 3b**). In other words, the roughness of the phase interface between PDMS and acrylate copolymers is thicker in PDMS-γCD-AAl ⊃ P(EA-HEMA) (*x*) than in PDMS-AAl/P(EA-HEMA) (*x*). At high *x* values, scattering characteristics from the spherical structures were observed in the same manner as in PDMS-γCD-AAl ⊃ P(EA-HEMA) (*x*); however, the diameters and distributions of spheres were assumed to be larger than those in PDMS-γCD-AAl ⊃ P(EA-HEMA) (*x*). Regarding scattering in the SAXS region ($q > 10^{-1}$ nm^{-1}), PDMS-γCD-AAl ⊃ P(EA-HEMA) (*x*) and PDMS-AAl/P(EA-HEMA) (*x*) both showed significant peaks at approximately $q = 0.4$ nm^{-1}, corresponding to the correlation between the PDMS phase and the acrylate copolymer phase. The scattering from the aggregation of γCD observed at the same q range (**Fig. S13**) as reported in our previous study[42]. The domain size (*d*) characterized the distance between neighbouring PDMS and acrylate copolymer domains estimated from the *q* value at the peak top. The details of the analytical methods are presented in the Supporting Information of section 6, and the *q* values estimated the *d* are listed in **Table S2**. In contrast, the SAXS profile of PDMS-AAl/P(EA-HEMA) (*x*) with a high *x* value did not exhibit a peak. The *d* values at each *x* are listed in **Table 1**. The *d* of PDMS-γCD-AAl ⊃ P(EA-HEMA) (*x*) was maximal at *x* = 20 mol% and then decreased

Table 1 Relationship between the molar ratio of HEMA (*x*) and the domain space (*d*) of the bicontinuous phase structure.

HEMA ratio, *x* [mol%]	Domain size *d* [nm]	
	with CD	without CD
0	16.0	17.9
20	21.6	24.9
43	20.7	24.6
70	15.5	N/A
100	14.0	N/A

with increasing *x*. The values of *d* at *x* value ranging from 0 to 43 mol% were larger for PDMS-AAl/P(EA-HEMA) (*x*) than for PDMS-γCD-AAl ⊃ P(EA-HEMA) (*x*). PDMS-γCD-AAl ⊃ P(EA-HEMA) (*x*), which became turbid above *x* = 43 mol% in visual observation, formed smaller phase structures than did PDMS-AAl/P(EA-HEMA) (*x*). Both visual and X-ray scattering measurements revealed that the movable crosslinks improved the compatibility between organic and inorganic polymers. Furthermore, a new correlation was observed near q = 0.1 nm^{-1} at relatively high *x* (the arrow symbol in **Fig. 3a** and **3b**). The organic–inorganic hybrid elastomers incorporated in this study had hierarchical phase structures on different size scales.

2.3. Effects of movable and reversible crosslinks on mechanical properties

The mechanical properties of PDMS-γCD-AAl ⊃ P(EA-HEMA) (*x*) and PDMS-AAl/P(EA-HEMA) (*x*) were evaluated through tensile tests. The stress-strain (S–S) curves of each elastomer with *x* = 0 mol% are shown in **Fig. 4a**. The vertical and horizonal axes are engineering stress and strain, respectively. PDMS-γCD-AAl ⊃ P(EA-HEMA) (0) exhibited a higher tensile strength and elongation at break than PDMS-AAl/P(EA-HEMA) (0). The initial slopes of the S–S curves were defined as the Young's moduli. The toughness was calculated from the area between the S–S curves and strain axis. The relationship between the Young's modulus and toughness is shown in **Fig. 4b**.

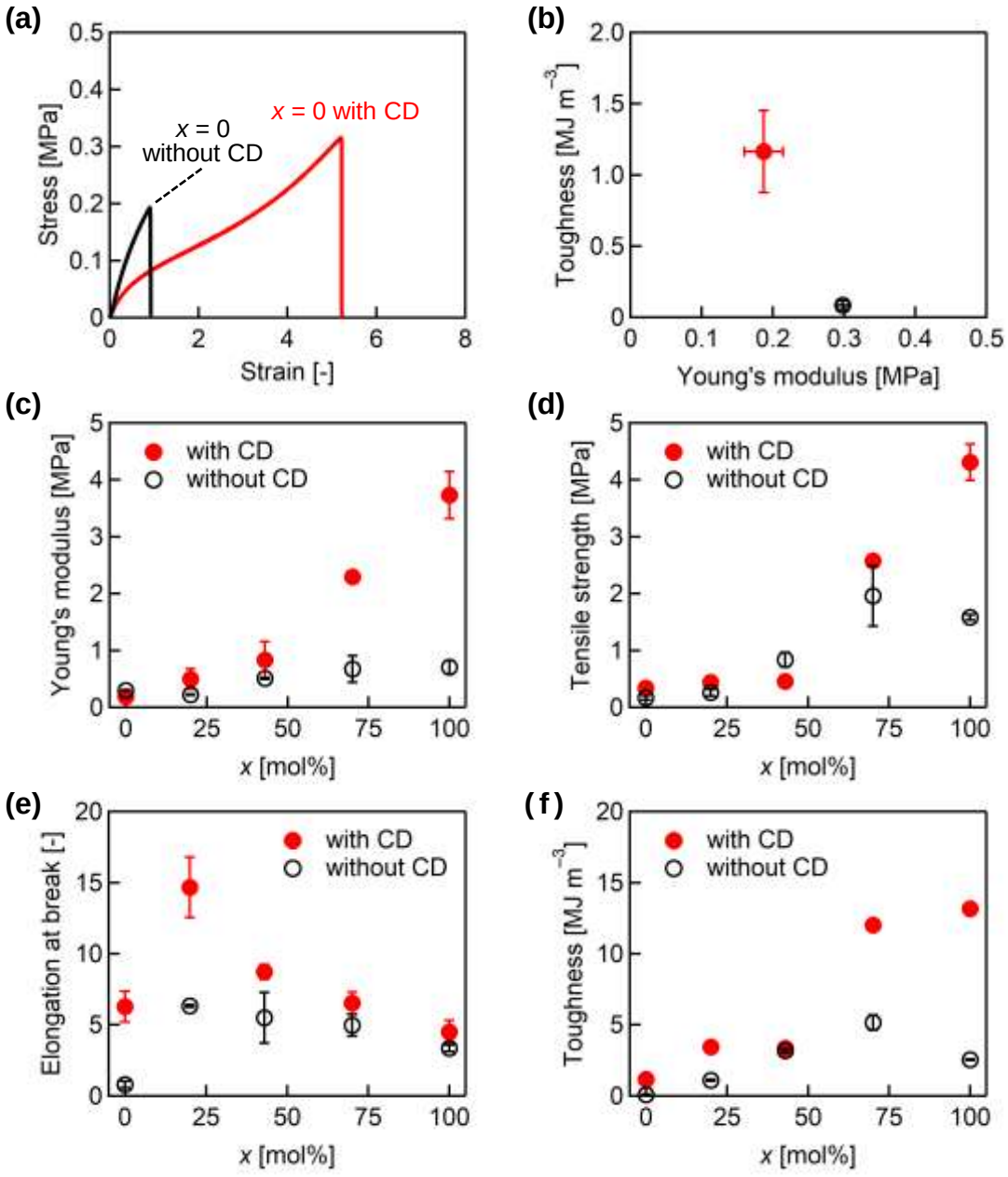

Fig. 4 (**a**) Stress–strain curve and (**b**) relationship between the toughness and Young's modulus of PDMS-γCD-AAl ⊃ P(EA-HEMA) and PDMS-AAl/P(EA-HEMA) at *x* = 0. Dependence of (**c**) Young's modulus, (**d**) tensile strength, (**e**) elongation at break, and (**f**) toughness on *x*.

Introducing movable crosslinks between PDMS and EA with γCDs improved the toughness values owing to the increases of tensile strength and elongation. In addition, the rough interface between PDMS and EA in PDMS-γCD-AAl ⊃ P(EA-HEMA) (0) observed by SAXS improved the toughness by inhibiting fracture at the phase interface. The Young's modulus decreased according to a general correlation between Young's modulus and toughness[49]. Based on rotaxane structures, slide and movable crosslinks have been reported for carbon-[50-56] and PDMS-based[42] materials, suggesting probable movable crosslinks involving γCDs in organic–inorganic hybrid materials.

The S–S curves of all the samples are shown in **Fig. S14**. We analysed these curves to evaluate certain mechanical properties, such as Young's modulus, tensile strength, elongation at break, and toughness. All the specimens fractured at the maximum stress. Cyclic tensile tests were performed to confirm the formation of movable crosslinks (**Fig. S15**). PDMS-γCD-AAl ⊃ P(EA-HEMA) (*x*) exhibited a large hysteresis loss similar to that of previously reported polymeric materials consisting of movable crosslinks[57] (**Fig. S16**).

The dependence levels of the HEMA content (*x*) on the Young's modulus, tensile strength, elongation at break, and toughness are shown in **Fig. 4c**, **4d**, **4e**, and **4f**, respectively. The formation of H-bonds was confirmed by Fourier-transform infrared spectroscopy (FT-IR). Increasing *x* formed more H-bonds. (**Fig. S17** and **S18**) The Young's modulus and tensile strength values of hybrid materials with γCD increased significantly with increasing *x*. Conversely, the elongation at break was maximized when *x* = 20 mol%; then, it decreased with increasing *x*. The largest elongation at *x* = 20 mol% can be explained by the polymer dynamics with microphase-separated dynamic bonds[58,59]. Reforming the H-bond pulled out in the other phase inhibits fracture at the phase interface and improves the elongation at break. However, the high-*x* elastomers broke at the interface of the macroscopic phase separation structure between PDMS and acrylate copolymers. The toughness values of the hybrid materials with γCD significantly increased with increasing *x*. Increasing the total number of crosslink points and introducing reversible crosslinks improved the mechanical strength characteristics (Young's modulus and tensile strength). However, excess reversible crosslinks decreased the elongation. Nonetheless, the toughness of PDMS-γCD-AAl ⊃ P(EA-HEMA) (*x*) was substantially higher than that of PDMS-AAl/P(EA-HEMA) (*x*) when *x* = 70 mol% or 100 mol%. The similarity tendency between the toughness and the mechanical strength in which they increased with increasing *x* indicated that the mechanical strength was the primary factor influencing the toughness of this hybrid material.

2.4. Mobility of acrylate copolymers

We investigated the thermal properties of PDMS-γCD-AAl ⊃ P(EA-HEMA) (*x*) to evaluate H-bond formation between dissimilar polymers. The glass transition temperature (T_g) of each polymer was measured by differential scanning calorimetry (DSC) (**Fig. S19**). All samples showed T_g values of approximately 153 K, thereby ascribing them as PDMS. PDMS was in a rubber state at the tensile test temperature. Therefore, we focused on the T_g values of acrylate copolymers to consider the relationship between the mechanical properties of the hybrid materials and the chain mobility. The T_g values of acrylate copolymers in hybrid materials (T_g^{DSC}) were observed to range from 250 K to 325 K, and they increased with increasing *x*. We estimated the T_g of only the acrylate copolymer according to the Fox equation (T_g^F) and evaluated the H-bond formation characteristics between dissimilar polymers. The ratio of T_g^{DSC} to T_g^F (T_g^{DSC}/T_g^F) was plotted against *x* in **Fig. 5**. When T_g^{DSC}/T_g^F was 1, T_g^{DSC} and T_g^F were equal. This finding suggested that H-bonds did not form between dissimilar polymers. The fact that T_g^{DSC} was higher than T_g^F indicated that the acrylate polymers formed H-bonds with PDMS at *x* = 20 mol% or 43 mol%. These compositions compounded the PDMS and acrylate copolymers at the nanoscale, as confirmed by SAXS. High compatibility levels could form reversible crosslinks between dissimilar polymers. The reversible crosslinks between dissimilar polymers acted upon a sacrificial bond and improved the elongation properties. At a high *x* value, PDMS and acrylate copolymers formed a macroscopic phase structure and did not bind each other with H-bonds. Therefore, the reversible crosslinks between acrylate copolymers inhibited the mobility levels of movable crosslinks and reduced the elongation properties.

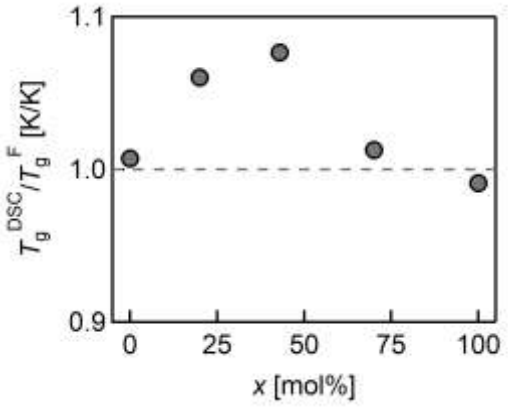

Fig. 5 Dependence of x on the ratio of the glass transition temperature obtained by DSC (T_g^{DSC}) and estimated by Fox Eq. (T_g^F) of the acrylate copolymers.

2.5. Mobility of movable crosslinks

Since the results of the tensile test implied changes in the mobility levels of movable crosslinks with the introduction of reversible crosslinks, we conducted stress relaxation tests. The specimens were stretched until a preset strain was reached, and they were held for 1000 s. The stress relaxation behaviours were plotted against the normalized stress, as shown in **Fig. S20** and **S21**. To quantitatively evaluate the stress relaxation behaviours, we attempted to fit the stress relaxation curves based on Kohlrausch–Williams–Watts (KWW) models. The fitting parameters of the KWW model are listed in **Table S4** and **S5**. Herein, we focused on the relaxation time (τ) in **Table 2**. PDMS-AAl/P(EA-HEMA) (*x*) had a large τ value at a low reversible crosslinks content. T_g of acrylate copolymers at the low *x* values was lower than the tensile tests temperature. The acrylate copolymers are in a rubber state when performing the tensile tests. Therefore, PDMS-AAl/P(EA-HEMA) (*x*) exhibited slow relaxation owing to the disentanglement of the backbone chain when *x* was small. At the high *x* values, T_g of acrylate copolymers was higher than the tensile tests temperature. The relaxation behaviour of backbone chains did not occur, and stresses were relaxed only in a short time. Conversely, PDMS-γCD-AAl ⊃ P(EA-HEMA) (*x*) exhibited a relatively fast stress relaxation behaviour

Table 2 The relaxation time was determined by fitting the KWW model.

HEMA ratio, *x* [mol%]	Relaxation time [s]	
	with CD	without CD
0	27	N/A
20	24	417
43	50	168
70	61	88
100	78	73

originating from the slide of movable crosslinks. Introducing reversible crosslinks increased the τ value and led to suggestion that the reversible crosslinks formed between acrylate polymers reduced the slide of movable crosslinks.

Increasing the content of reversible crosslinks improved the mechanical strength properties, such as Young's modulus and tensile strength, because the number of crosslinking points increased and reducing the mobility of movable crosslinks was reduced.

3. Conclusions

We successfully composited organic–inorganic hybrid materials (PDMS-γCD-AAl ⊃ P(EA-HEMA) (*x*)) by incorporating TAcγCD-originating movable crosslinks between PDMS and acrylate polymers. Introducing reversible crosslinks based on H-bonds improved the mechanical properties of the hybrid materials. The Young's modulus increased because of an increase in the total number of crosslinking points. The elongation properties were enhanced by reversible crosslinks between dissimilar polymers because reforming the reversible crosslinks at the interface of microscopic phase structure inhibited the fracture of the interface. Excess introduction of the H-bond moiety induced macroscopic phase separation and decreased the elongation at break. The slide of movable crosslinks was inhibited due to the formation of reversible crosslinks between acrylate polymers and increased Young's modulus and tensile tests. The toughness of PDMS-γCD-AAl ⊃ P(EA-HEMA) (*x*) was much higher than that of PDMS-AAl/P(EA-HEMA) (*x*). The toughness values of these hybrid materials were strongly affected by their Young's moduli.

PDMS materials have been applied in various fields because of their transparency levels. A challenge limiting applicability of PDMS is its poor mechanical properties. Our material designs incorporated cooperatively movable crosslinks to achieve highly compatible immiscible polymers. We expect this report to be a pioneering work in regard to overcoming the limitations of topological crosslinks towards composites of incompatible polymer blends.

Author Contributions

N.Y.: Data curation; Formal analysis; Investigation; Visualization. K.Y.: Data curation; Formal analysis; Investigation; Writing – original draft. R.I.: Investigation. D.Y.: Methodology. J.P.: Investigation. H.N.: Resources. Y.T.: Conceptualization; Funding acquisition; Project administration; Supervision. All authors critically reviewed and edited the manuscript draft and approved the final version for submission.

Conflicts of interest

There are no conflicts to declare.

Acknowledgements

This work was supported by Japan Science and Technology Agency (JST), the Core Research for Evolutional Science and Technology (CREST) program JPMJCR22L4 (Y.T.), COI-NEXT program JPMJPF2218, the Asahi Glass Foundation, the Yazaki Memorial Foundation for Science, and the establishment of university fellowships towards the creation of science technology innovation, grant number JPMJFS2125 (D.Y.). The authors would like to thank Dr Keiichi Osaka, Dr Noboru Ohta, and Yuka Ikemoto in Japan Synchrotron Radiation Research Institute (JASRI) for the synchrotron radiation measurements. Synchrotron radiation experiments were performed at BL19B2, BL40B2, and BL43IR of SPring-8 with the approval of JASRI (Proposal Nos. 2022B1704, 2022B1705, and 2022B1934). We thank Dr. Naoya Inazumi and the Analytical Instrumental Facility, Graduate School of Science, Osaka University, for supporting NMR measurements and FT-IR spectroscopy.

References

1 G. Keledi, J. Hári and B. Pukánszky, *Nanoscale*, 2012, **4**, 1919-1938.
2 S. Kango, S. Kalia, A. Celli, J. Njuguna, Y. Habibi and R. Kumar, *Prog. Polym. Sci.*, 2013, **38**, 1232-1261.
3 Y. Jeon, S. Nagappan, X.-H. Li, J.-H. Lee, L. Shi, S. Yuan, W.-K. Lee and C.-S. Ha, *ACS Appl. Mater. Interfaces*, 2021, **13**, 6615-6630.
4 J. I. Weon and H. J. Sue, *Polymer*, 2005, **46**, 6325-6334.
5 D.-R. Yei, H.-K. Fu, Y.-H. Chang, S.-W. Kuo, J.-M. Huang and F.-C. Chang, *J. Polym. Sci., Part B: Polym. Phys.*, 2007, **45**, 1781-1787.
6 M. Bhattacharya, S. Biswas, S. Bandyopadhyay and A. K. Bhowmick, *Polym. Adv. Technol.*, 2012, **23**, 596-610.
7 M. Kotal and A. K. Bhowmick, *Prog. Polym. Sci.*, 2015, **51**, 127-187.
8 Y.-Y. Yu and W.-C. Chen, *Mater. Chem. Phys.,* 2003, **82**, 388-395.
9 S. Sugimoto, M. Inutsuka, D. Kawaguchi and K. Tanaka, *Polym. J.*, 2020, **52**, 217-223.
10 G. Park, H. Lee, J. H. Sim, A. Kim, M. Kim and K. Paeng, *J. Colloid Interface Sci.*, 2023, **629**, 256-264.
11 N. Cioffi, L. Torsi, N. Ditaranto, G. Tantillo, L. Ghibelli, L. Sabbatini, T. Bleve-Zacheo, M. D'Alessio, P. G. Zambonin and E. Traversa, *Chem. Mater.*, 2005, **17**, 5255-5262.
12 W. Shao, D. Nabb, N. Renevier, I. Sherrington, Y. Fu and J. Luo, *J. Electrochem. Soc.*, 2012, **159**, D671.
13 A. Słubik, A. Smejda-Krzewicka and K. Strzelec, *Polymers*, 2021, **13**, 853.
14 G. Cardoen and E. B. Coughlin, *Macromolecules*, 2004, **37**, 5123-5126.
15 S.-W. Kuo and F.-C. Chang, *Prog. Polym. Sci.*, 2011, **36**, 1649-1696.

16 Y.-F. Zhu, W. Liu, M.-Y. Zhang, Y. Zhou, Y.-D. Zhang, P.-P. Hou, Y. Pan, Z. Shen, X.-H. Fan and Q.-F. Zhou, *Macromolecules*, 2015, **48**, 2358-2366.
17 H. Blattmann and R. Mülhaupt, *Macromolecules*, 2016, **49**, 742-751.
18 W. Zhang, G. Camino and R. Yang, *Prog. Polym. Sci.*, 2017, **67**, 77-125.
19 A. Takahashi, T. Okada, K. Nakano, Y. Ishida and A. Kameyama, *Polym. J.*, 2021, **53**, 1213-1222.
20 T. Nakano, K. Okamoto, H. Imoto and K. Naka, *Polym. J.*, 2023, **55**, 193-201.
21 G. Camino, S. M. Lomakin and M. Lazzari, *Polymer*, 2001, **42**, 2395-2402.
22 G. Camino, S. M. Lomakin and M. Lageard, *Polymer*, 2002, **43**, 2011-2015.
23 T. S. Radhakrishnan, *J. Appl. Polym. Sci.*, 2006, **99**, 2679-2686.
24 H. N. Apostoleris, M. Chiesa and M. Stefancich, *J. Mater. Chem. C*, 2015, **3**, 1371-1377.
25 T. M. Reidy, D. Luo, P. Rana, B. Huegel and X. Cheng, *J. Micromech. Microeng.*, 2019, **29**, 015014.
26 M. Ionescu, B. Winton, D. Wexler, R. Siegele, A. Deslantes, E. Stelcer, A. Atanacio and D. D. Cohen, *Nucl. Instrum. Methods Phys. Res., Sect. B*, 2012, **273**, 161-163.
27 I. Miranda, A. Souza, P. Sousa, J. Ribeiro, E. M. S. Castanheira, R. Lima and G. Minas, *J. Funct. Biomater.*, 2022, **13**, 2.
28 C. M. Yun, Y. Nagase and M. Nakagawa, *Mol. Cryst. Liq. Cryst.*, 2013, **580**, 35-38.
29 C. M. Yun, E. Akiyama, T. Yamanobe, H. Uehara and Y. Nagase, *Polymer*, 2016, **103**, 214-223.
30 R. M. Kappel, A. J. H. Klunder and G. J. M. Pruijn, *Eur. J. Plast. Surg.*, 2014, **37**, 123-128.
31 M. Mizuno, M. Takahashi, Y. Tokuda and T. Yoko, *Chem. Mater.*, 2006, **18**, 2075-2080.
32 M. Vatankhah-Varnosfaderani, A. N. Keith, Y. Cong, H. Liang, M. Rosenthal, M. Sztucki, C. Clair, S. Magonov, D. A. Ivanov, A. V. Dobrynin and S. S. Sheiko, *Science*, 2018, **359**, 1509-1513.
33 X. Wang, S. Zhan, Z. Lu, J. Li, X. Yang, Y. Qiao, Y. Men and J. Sun, *Adv. Mater.*, 2020, **32**, 2005759.
34 S. Yu, H. Zuo, X. Xu, N. Ning, B. Yu, L. Zhang and M. Tian, *ACS Appl. Polym. Mater.*, 2021, **3**, 2667-2677.
35 C.-L. He, F.-C. Liang, L. Veeramuthu, C.-J. Cho, J.-S. Benas, Y.-R. Tzeng, Y.-L. Tseng, W.-C. Chen, A. Rwei and C.-C. Kuo, *Adv. Sci.*, 2021, **8**, 2102275.
36 J. Li, H. Niu, Y. Yu, Y. Gao, Q. Wu, F. Wang and P. Sun, *ACS Appl. Polym. Mater.*, 2021, **3**, 3373-3382.
37 J. Mo, X. Chen, Y. Fu, R. Li, Y. Lin and A. Zhang, *Polymer*, 2021, **228**, 123903.
38 P. Hu, J. Madsen and A. L. Skov, *Nat. Commun.*, 2022, **13**, 370.
39 K. Cheng, A. Chortos, J. A. Lewis and D. R. Clarke, *ACS Appl. Mater. Interfaces*, 2022, **14**, 4552-4561.
40 E. Dashtimoghadam, M. Maw, A. N. Keith, F. Vashahi, V. Kempkes, Y. D. Gordievskaya, E. Y. Kramarenko, E. A. Bersenev, E. A. Nikitina, D. A. Ivanov, Y. Tian, A. V. Dobrynin, M. Vatankhah-Varnosfaderani and S. S. Sheiko, *Mater. Horiz.*, 2022, **9**, 3022-3030.
41 D. Yoshida, J. Park, R. Ikura, N. Yamashita, H. Yamaguchi and Y. Takashima, *Chem. Lett.*, 2022, **52**, 93-96.
42 D. Yoshida, J. Park, N. Yamashita, R. Ikura, N. Kato, M. Kamei, K. Ogura, M. Igarashi, H. Nakagawa and Y. Takashima, *Polym. Chem.*, 2023, **14**, 3277-3285.
43 R. Ikura, S. Murayama, J. Park, Y. Ikemoto, M. Osaki, H. Yamaguchi, A. Harada, G. Matsuba and Y. Takashima, *Mol. Syst. Des. Eng.*, 2022, **7**, 733-745.
44 R. Ikura, J. Park, M. Osaki, H. Yamaguchi, A. Harada and Y. Takashima, *NPG Asia Mater.*, 2022, **14**, 10.
45 Y. Kawai, J. Park, Y. Ishii, O. Urakawa, S. Murayama, R. Ikura, M. Osaki, Y. Ikemoto, H. Yamaguchi, A. Harada, T. Inoue, H. Washizu, G. Matsuba and Y. Takashima, *NPG Asia Mater.*, 2022, **14**, 32.
46 Y. Kawai, J. Park, S. Murayama, R. Ikura, M. Osaki, T. Konishi, G. Matsuba and Y. Takashima, *Macromolecules*, 2023, **56**, 4503-4512.
47 E. Dashtimoghadam, M. Maw, A. N. Keith, F. Vashahi, V. Kempkes, Y. D. Gordievskaya, E. Y. Kramarenko, E. A. Bersenev, E. A. Nikitina, D. A. Ivanov, Y. Tian, A. V. Dobrynin, M. V-. Varnosfaderani and S. S. Sheiko, *Mater. Horiz.*, 2022, **9**, 3022-3030.
48 A. J. Silvaroli, T. R. Heyl, Z. Qiang, J. M. Beebe, D. Ahn, S. Mangold, K. R. Shull and M. Wang, *ACS Appl. Mater. Interfaces*, 2020, **12**, 44125-44136.
49 C. E. Carraher, in *Carraher's Polymer Chemistry*, CRC Press, Boca Raton, Florida, 10th ed., 2017, chap. 14th, pp. 544-566.
50 Y. Okumura and K. Ito, *Adv. Mater.*, 2001, **13**, 485-487.
51 K. Koyanagi, Y. Takashima, H. Yamaguchi and A. Harada, *Macromolecules*, 2017, **50**, 5695-5700.
52 J. Sawada, D. Aoki, Y. Sun, K. Nakajima and T. Takata, *ACS Appl. Polym. Mater.*, 2020, **2**, 1061-1064.
53 C. Liu, N. Morimoto, L. Jiang, S. Kawahara, T. Noritomi, H. Yokoyama, K. Mayumi and K. Ito, *Science*, 2021, **372**, 1078-1081.
54 C. Jin, J. Park, H. Shirakawa, M. Osaki, Y. Ikemoto, H. Yamaguchi, H. Takahashi, Y. Ohashi, A. Harada, G. Matsuba and Y. Takashima, *Soft Matter*, 2022, **18**, 5027-5036.
55 Z. Zhu, S. West, H. Chen, G.-H. Lai, S. Uenuma, K. Ito, M. Kotaki and H.-J. Sue, *ACS Appl. Polym. Mater.*, 2023, **5**, 3971-3978.
56 Z. Zhu, H. Chen, X. Zhu, Z. Sang, S. A. Sukhishvili, S. Uenuma, K. Ito, M. Kotaki and H.-J. Sue, *Compos. Sci. Technol.*, 2023, **235**, 109976.
57 R. Ikura, J. Park, M. Osaki, H. Yamaguchi, A. Harada and Y. Takashima, *Macromolecules*, 2019, **52**, 6953-6962.
58 S. Ge, S. Samanta, B. Li, G. P. Carden, P. F. Cao and A. P. Sokolov, *ACS Nano*, 2022, **16**, 4746-4755.
59 P. Carden, S. Ge, S. Zhao, B. Li, S. Samanta and A. P. Sokolov, *Macromolecules*, 2023, **56**, 5173–5180.